Electronic Supplementary Information (ESI)

Asymmetric allyl-activation of organosulfides for high-energy reversible redox flow batteries

Guo-Ming Weng,‡[a] Bin Yang,‡[a] Chi-You Liu,[b] Guan-Ying Du,[b] Elise Y. Li[b,*] and Yi-Chun Lu[a,*]

[a]Electrochemical Energy and Interfaces Laboratory, Department of Mechanical and Automation Engineering, The Chinese University of Hong Kong, Shatin, N. T. 999077, Hong Kong

[b]Department of Chemistry, National Taiwan Normal University, No. 88, Section 4, Tingchow Road, Taipei 116, Taiwan

‡G. M. W. and B. Y. contributed equally to this work.

E-mail: yichunlu@mae.cuhk.edu.hk / eliseytli@ntnu.edu.tw

Experimental section

Materials. 1,2-dimethoxyethane (DME, 99.5%), 1,3-Dioxolane (DOL, 99.5%), *N*,*N*′-dimethylformamide (DMA,99.8%), LiTFSI (99.95%), lithium bis(trifluoromethane) sulfonamide (LiTFSI,99.95%), lithium nitrate ($LiNO_3$, 99.99%) were received from Sigma-Aldrich. Diallyl disulfide (DDS, >80%), bis(3-fluorophenyl) disulfide (FDS, >97.0%), diphenyl disulfide (PDS, >99%), di(4-aminophenyl) disulfide (MDS, >98%) were received from TCI Chemicals. Diallyl trisulfide (DTS, 98%) was received from AIKE Reagent, China. PVDF powder (#140618) was received from Shenzhen Kejing of MTI Corp. LITHion™ Dispersion (lithiated Nafion polymer in isopropyl alcohol) was received from Ion Power Inc., US. Carbon paper (HCP020N) was received from Shanghai Hesen Electric Co. Ltd. Lithium foil was received from Shenzhen Meisen Electro-mechanical Co. Ltd. $LiNO_3$ and LiTFSI were dried overnight under dynamic vacuum in a glass oven (Büchi, Switzerland) at 110 ℃.

Preparation and assembly of nonaqueous lithium/organosulfides battery (LOB). The configuration and the components of a nonaqueous lithium/organosulfides battery (LOB) are shown in the Supplementary Fig. 2 and described in our previous works[1-3]. To assembly the LOB with LAGP electrolyte: i) lithium foil (Φ16 mm) was immersed in 0.1 M $LiNO_3$ of DOL:DME (1:1 v:v) overnight before use; ii) one piece of lithium foil was pressed onto the surface of the stainless steel bottom casing; iii) total 120 µL anolyte, 1 M LiTFSI-0.4 M $LiNO_3$ in DOL:DME (1:1 v:v), was added on the lithium foil; iv) two Celagrd 2325 (Φ19 mm) was placed onto the lithium foil followed by LAGP solid electrolyte[3, 4] (*Φ*19 mm). v) one piece of carbon paper (Φ 12 mm) was placed onto the LAGP to serve as both positive electrode and buffer layer; vi) 10 µL catholyte was added onto this carbon paper; vii) additional piece of carbon paper was placed on the 1st carbon paper to act as current collector followed by a stainless steel spring; viii) two casings (bottom and top) were separated by a spacer and the assembly was conducted in the Ar-filled glove box (Etelux, H_2O < 1.0 ppm, O_2 < 1.0 ppm). The catholytes include single component (i.e. 2.5 M MDS/PDS/FDS/DDS/DTS) and mixed organosulfides (i.e. 2.5 M DDS+2.5 M MDS/PDS/FDS and 2.5 M DTS+2.5 M MDS/PDS/FDS) in 0.2 M LiTFSI-0.1 M $LiNO_3$ of DOL:DME (1:1 v:v), respectively. The

electrolytes were prepared by dissolving DDS, DTS, PDS, MDS, FDS, LiTFSI and $LiNO_3$ in the binary solvents of DOL and DME.

For the cell assembly with PNC separator, the two Celgards and one piece of LAGP was replaced with one PNC separator. The cells with PNC were left idle for 1 hour before test.

For the flow cell assemble, the cell photograph is shown in Supplementary Fig.2d. LAGP was used as separator due to the underlying low resistance of porous Celgard-based membrane in hydraulic crossover between the half-cells. 5 mL catholyte was contained in a reservoir.

Cyclic Voltammetry measurement. Cyclic voltammetry (CV) tests were conducted using a three-electrode configuration with carbon paper (CP) electrode as the working electrode, a platinum wire (diameter 0.5 mm) as the counter electrode and an Ag/Ag^+ reference electrode (Ag wire in a 0.01 M $AgNO_3$/0.1 M TBAP ACN solution, ALS CO., Ltd, Japan) as the reference electrode. The cell was assembled in Ar atmosphere. The concentration of active materials were 10 mM DTS, 10 mM PDS, 10 mM FDS, 10 mM DTS + 10 mM PDS and 10 mM DTS + 10 mM FDS in 1M LiTFSI-0.4 M $LiNO_3$ DOL:DME (v:v=1:1).

Preparation of PVDF-Nafion coated Celgard (PNC). 421 mg PVDF powder and 5 mL LITHion™ Dispersion were firstly dried overnight at 60 ℃ and added into 5 ml of DMA. The mixture solution was stirred vigorously and heated at 80 ℃ for 2 hours in an Ar-filled glove box until a clear solution was obtained. Then the above solution was cooled to room temperature. One piece of Celgard 2325 was immersed into the above solution and placed onto a petri dish, which was dried in an oven at 60 ℃ for 1 hour to remove the solvent. After the modified Celgard was cooled to room temperature, it was peeled off from the petri dish in DI water. The final product was dried in an oven at 60 ℃ overnight before use. The thickness of the coating film (onto each side of Celgard) is about 6 μm according to electron microscope characterization.

Test of static and flow batteries. Galvanostatic tests were carried out with a Bio-logic VMP3 potentiostat at ~20 ℃. The charge and discharge tests of the LOB are operated with constant current method (current density is based on the active geometric area of the electrode). The cutoff voltages for the typical charge and discharge cycle with LAGP separator at 0.1 mA cm^{-2} are 3 V and 1.7 V (3 V-1.6 V for MDS), while those with PNC separator at 1 mA cm^{-2} are 3 V and 1.5 V. The performance of the LOB in continuous flow mode was studied with LAGP at 0.1 mA cm^{-2}. The flow rate was 8 mL min^{-1}.

Computational method. Density functional theory (DFT) calculations of all molecules were performed by the Gaussian 09 program[5]. The geometries of all the molecules were calculated at the UM11[6]/6-311+G(d,p) level. The minima were confirmed with no imaginary frequencies. The implicit SMD[7] continuous solvation model for the tetrahydrofuran (THF) was adopted. In the DFT calculation, the solvent effect was considered by employing the implicit Solvation Model based on Density (SMD) but not the explicit solvent molecules since the S-S or C-S bond breakage is an intrinsic property and the surrounding solvent molecules are expected to have very small or negligible effect.

Characterization. GC-MS analysis was conducted with an Agilent 7890B gas chromatograph coupled to an Agilent 5977A mass spectrometer with a mass range m/z of 40 to 400 and a solvent delay of 2 mins (avoiding the overloaded solvent peak in the chromatograph). An Agilent J&W HP-5ms Ultra Inert GC Column (30 m by 0.25 mm, df = 0.25 μm) was used with helium as the carrier gas. Samples (diluted by acetonitrile) were injected (1 μL for each test) at 220 ℃ with a split ratio of 50:1, and the oven temperature was programmed to increase at 6 ℃ min^{-1} to 200 ℃ and held constant for 30 mins. The MS transfer line temperature was 230 ℃. Species were identified by matching sample mass spectrum with those of the National Institute of Standards and Technology (NIST) MS spectral library for peaks presented in the chromatograms. The PNC was characterized by the scanning electron microscopy (SEM) with a JSM-7800F Schottky Field Emission Scanning Electron Microscope. XPS experiments were performed using Thermo Fisher Scientific instrument equipped with focused monochromatic Al K (alpha) source. XPS spectra with the energy step of 0.05 eV were recorded using software SmartSoft-XPS v2.0 and processed

using CasaXPS software. The spectrum was calibrated setting its C1s binding energy (BE) to 284.8 eV and verified using adventitious (aliphatic) carbon (e.g. PET) BE. The XPS spectra were fitted using a combination of Gaussians and Lorentzians with 0–50% of Lorentzian contents. Shirley background was used for curve-fitting. The $S2p_{3/2}$ and $S2p_{1/2}$ doublets were constrained using peak areas of 2:1 with a splitting of 1.2 eV.

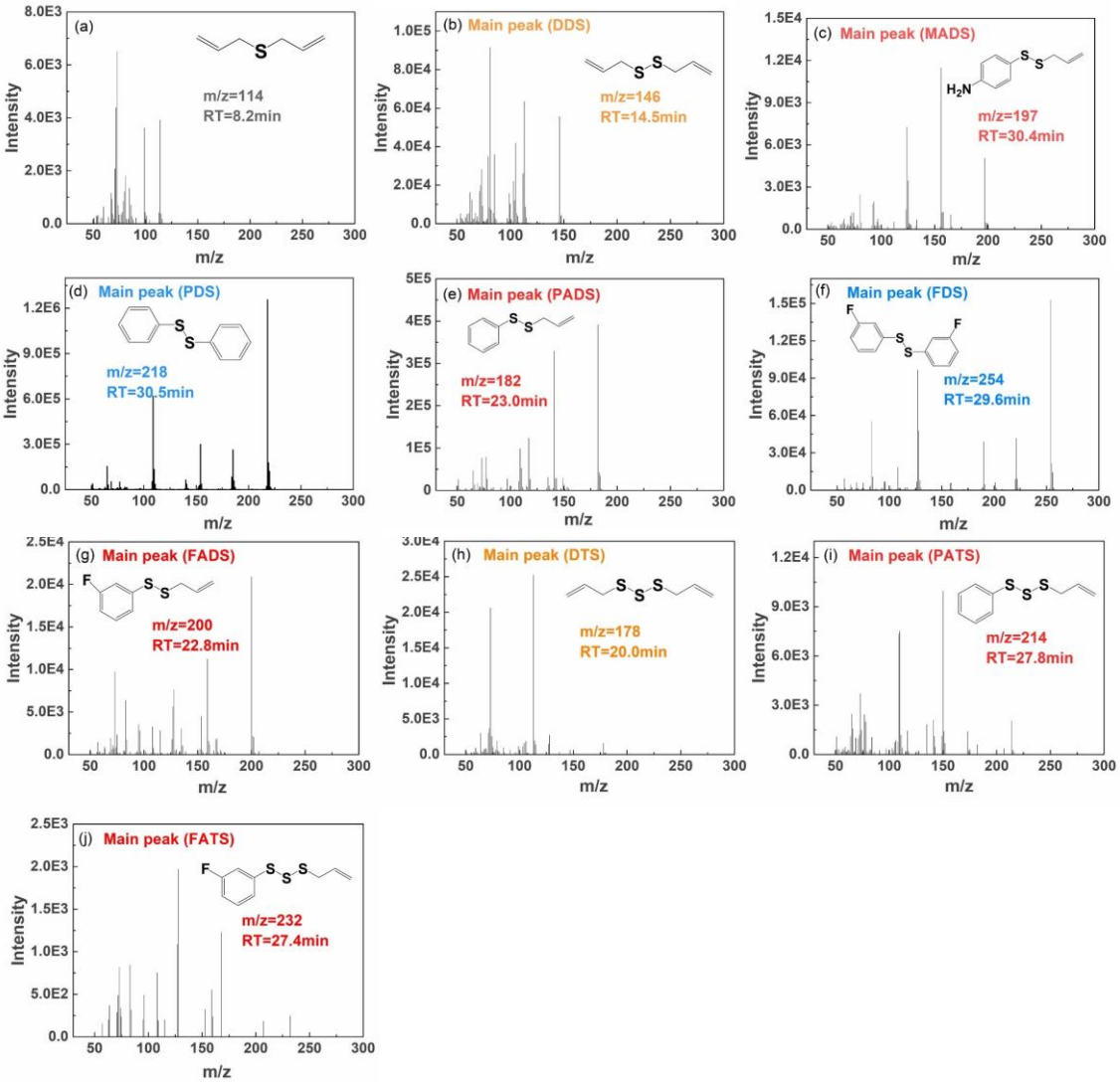

Fig. S1. Mass spectra of corresponding GC peaks shown in Fig. 2 in the main text.

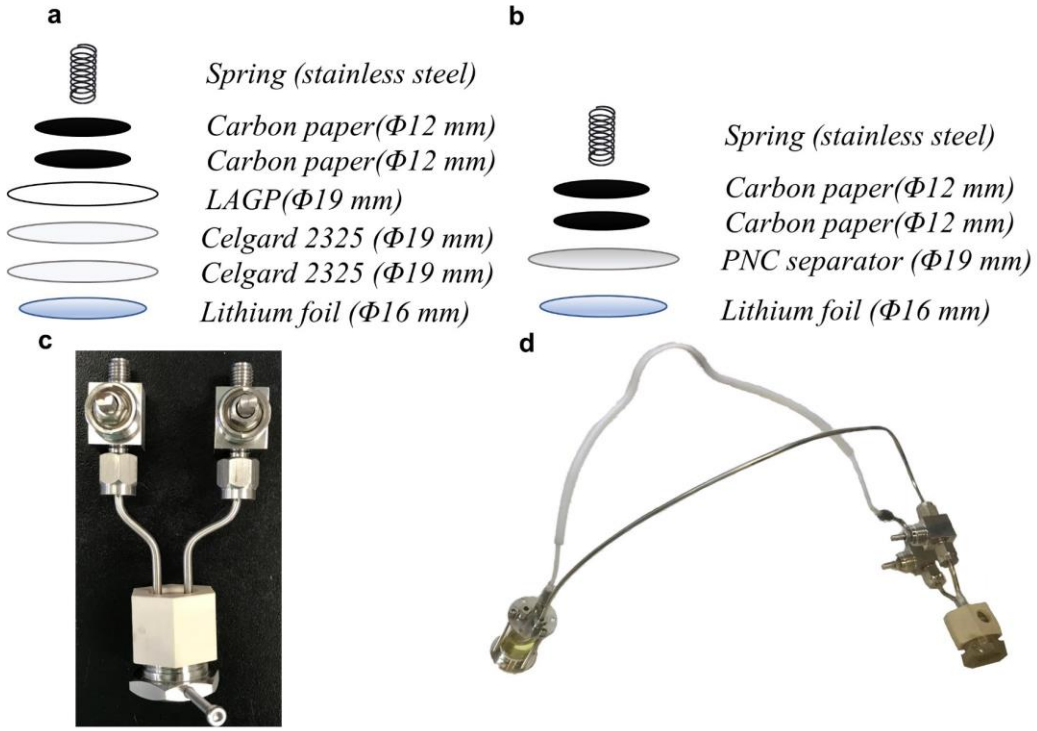

Fig. S2. Schematic representation of the proposed LOB cell configuration and photographs. Cell configuration **a)** with LAGP electrolyte at 0.1 mA cm^{-2}. b) with PNC separator at 1 mA cm^{-2}. Photographs of **c)** static cell **d)** flow cell.

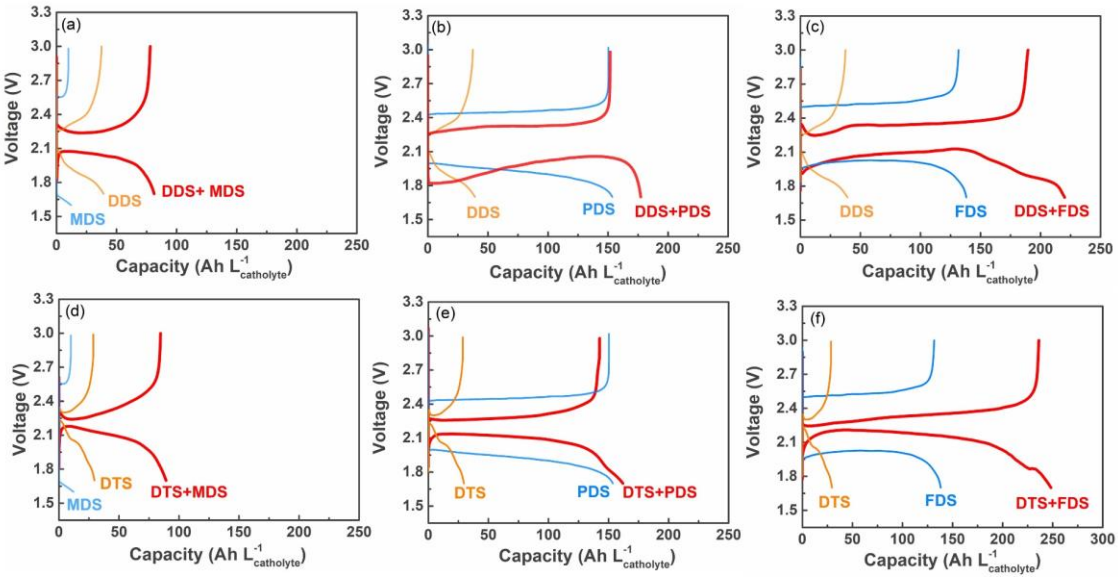

Fig. S3. Galvanostatic voltage profiles with different catholyte for the 1st cycle at 0.1 mA cm-2. **a**, DDS+MDS. **b**, DDS+PDS. **c**, DDS+FDS. **d**, DTS+MDS. **e**, DTS+PDS. **f**, DTS+FDS. The performance of the individual system under the same condition are included.

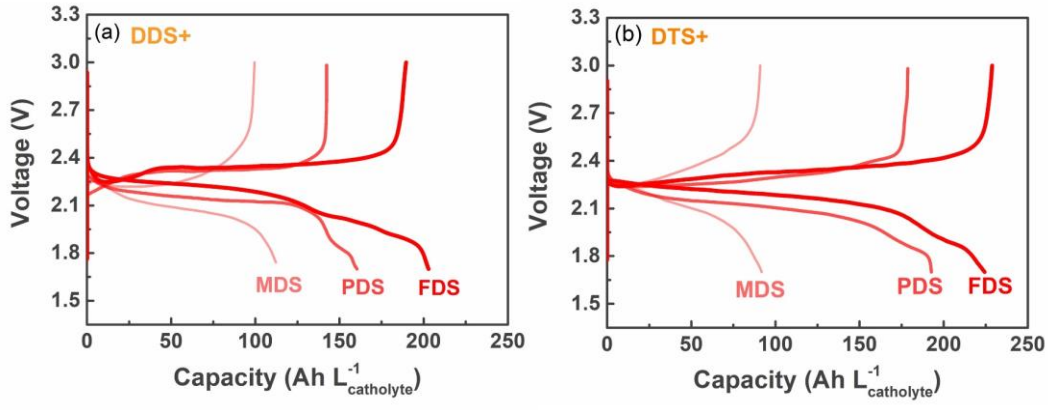

Fig. S4. Galvanostatic discharge and charge curves comparison. a, DDS mix with MDS, PDS and FDS. **b**, DTS mix with MDS, PDS and FDS. LAGP was used as the separator and the discharge and charge current density was 0.1 mA cm-2.

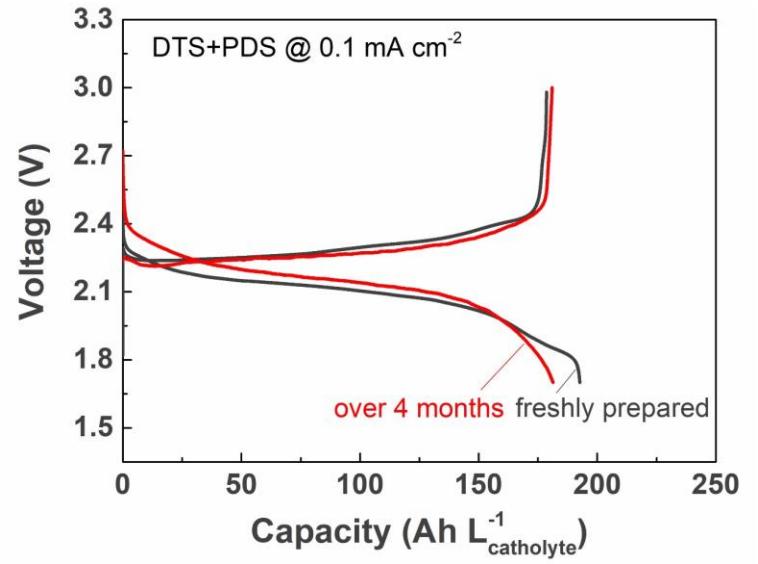

Fig. S5. The 2nd cycle of 2.5 M DTS+ 2.5 M PDS with different electrolyte mixing time at 0.1 mA cm^{-2}

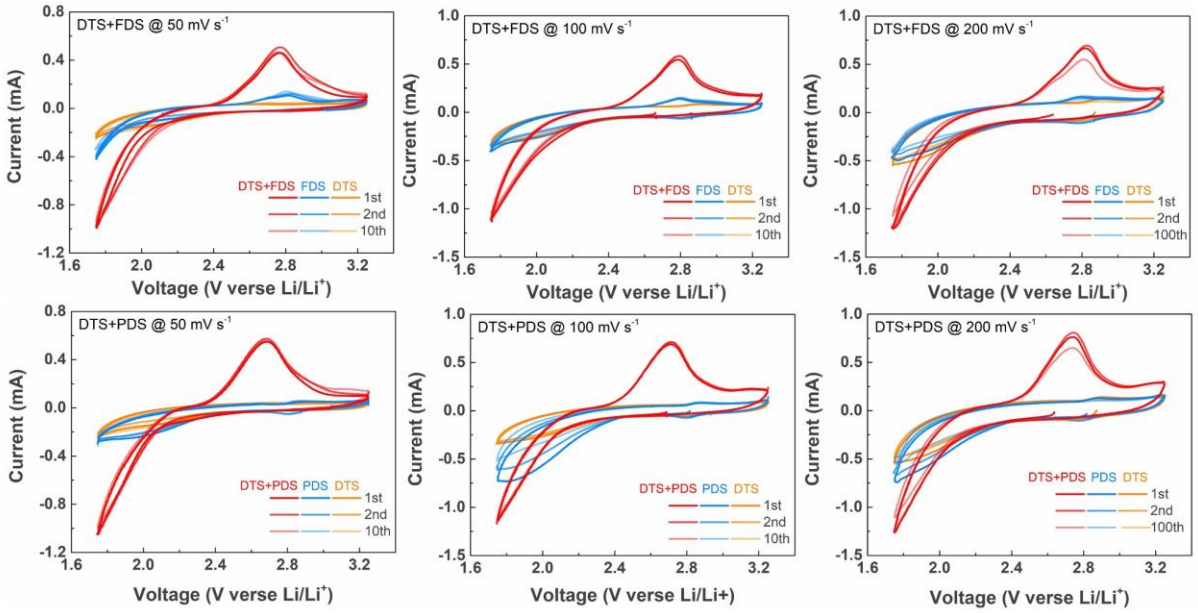

Fig. S6. CVs comparison for DTS-mixed systems (10 mM DTS+ 10 mM PDS ,10 mM DTS+10 mM FDS and 10 mM individual member included) at different scan rates.

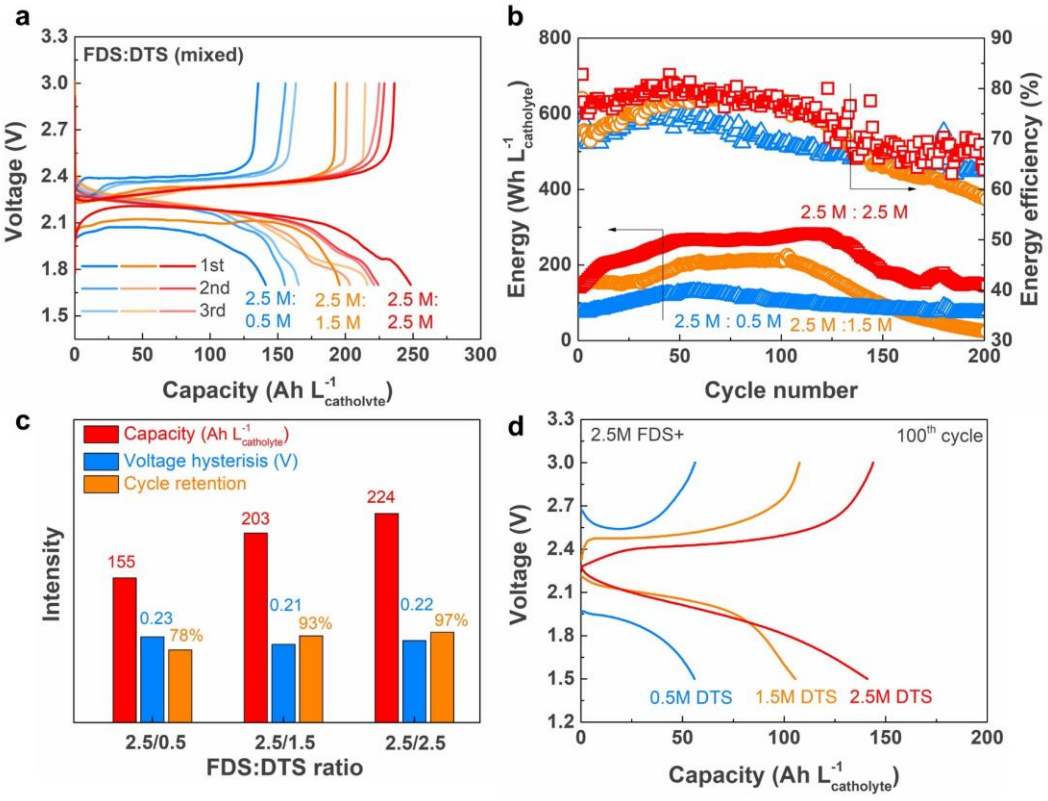

Fig. S7. FDS:DTS ratio effects on the electrochemical performance. a, the initial three cycles with LAGP membrane at 0.1 mA cm^{-2}. **b**, cycle stability of FDS: DTS system with PNC membrane at 1mA cm^{-2} **c,** capacity, voltage hysteresis and cycle retention comparison. Here we use the percentage (capacity at 100^{th} cycle/maximum capacity) to represent the cycle retention. d, discharge-charge profile at 100^{th} cycle from **b.**

Table S1. The bond lengths of the organosulfides (*d*, in Å). The schematic geometries show the selected bond by d_1, d_2, d_2', and d_3.

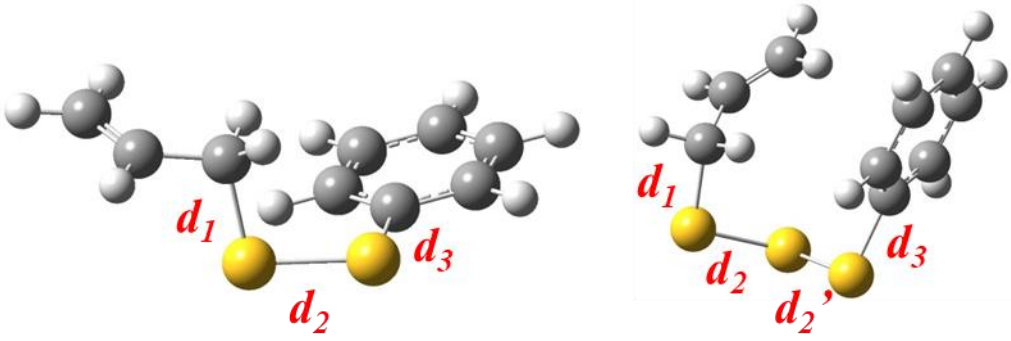

	d_1 (C-S)		d_2 (S-S)		d_3 (C-S)	
	Neutral	Anion	Neutral	Anion	Neutral	Anion
DDS	1.84	1.84	2.07	**2.79**	1.84	1.84
PDS	1.79	1.76	2.11	**2.83**	1.79	1.76
PADS	1.84	1.84	2.07	**2.80**	1.80	1.76

	d_1 (C-S)		d_2 (S-S)		d_2' (S-S)		d_3 (C-S)	
	Neutral	Anion	Neutral	Anion	Neutral	Anion	Neutral	Anion
DTS	1.84	1.84	2.08	2.07	2.08	**3.33**	1.84	1.84
PTS	1.80	1.84	2.07	2.05	2.09	**2.83**	1.79	1.79
PATS	1.84	1.84	2.07	2.05	2.09	**2.84**	1.79	1.79

Table S2. Calculated cleavage reaction energies (in eV) of disulfide- and trisulfide-based system.

R_1-S_2-R_2 $\xrightarrow[\text{THF}]{}$ **Products**

R_1	R_2	Products	ΔG (eV)	R_1	R_2	Products	ΔG (eV)
P	P	2PS•	**1.35**	P	A	[A• + PS_2•]	**1.33**
		[P• + PS_2•]	2.42			[PS• + AS•][a]	**1.56**
		[PS^- + PS^+]	3.84			[PS^- + AS^+][a]	2.33
		[P^+ + PS_2^-]	4.51			[P• + AS_2•]	2.36
		[P^- + PS_2^+]	5.77			[A^+ + PS_2^-]	2.97

A	A	[A• + AS_2•]	**1.30**			[PS^+ + AS^-]	4.19
		2AS•[a]	**1.80**			[P^+ + AS_2^-]	4.63
		[AS^- + AS^+][a]	2.71			[A^- + PS_2^+]	5.20
		[A^+ + AS_2^-]	3.12			[P^- + AS_2^+]	5.89
		[A^- + AS_2^+]	5.35				

R_1-S_3-R_2 $\xrightarrow[\text{THF}]{}$ Products

R_1	R_2	Products	ΔG (eV)	R_1	R_2	Products	ΔG (eV)
P	P	[PSS• + PS•]	**1.06**	P	A	[ASS• + PS•]	**1.08**
		[P• + PSSS•]	2.50			[PSS• + AS•][a]	**1.35**
		[PS^- + PSS^+]	3.48			[A• + PSSS•]	**1.48**
		[PSS^- + PS^+]	3.78			[PSS^- + AS^+][a]	2.34
		[P^+ + $PSSS^-$]	4.46			[P• + ASSS•]	2.50
		[P^- + $PSSS^+$]	5.91			[A^+ + $PSSS^-$]	2.99
A	A	[ASS• + AS•][a]	**1.26**			[PS^- + ASS^+]	3.67
		[A• + ASSS•]	**1.39**			[AS^- + PSS^+]	3.90
		[ASS^- + AS^+][a]	2.44			[ASS^- + PS^+]	3.97
		[A^+ + $ASSS^-$]	2.92			[P^+ + $ASSS^-$]	4.48
		[AS^- + ASS^+]	4.00			[A^- + $PSSS^+$]	5.42
		[A^- + $ASSS^+$]	5.29			[P^- + $ASSS^+$]	5.89

[a] The [AS•] and [AS^+] products refer to the more stable structures which are tautomerized.

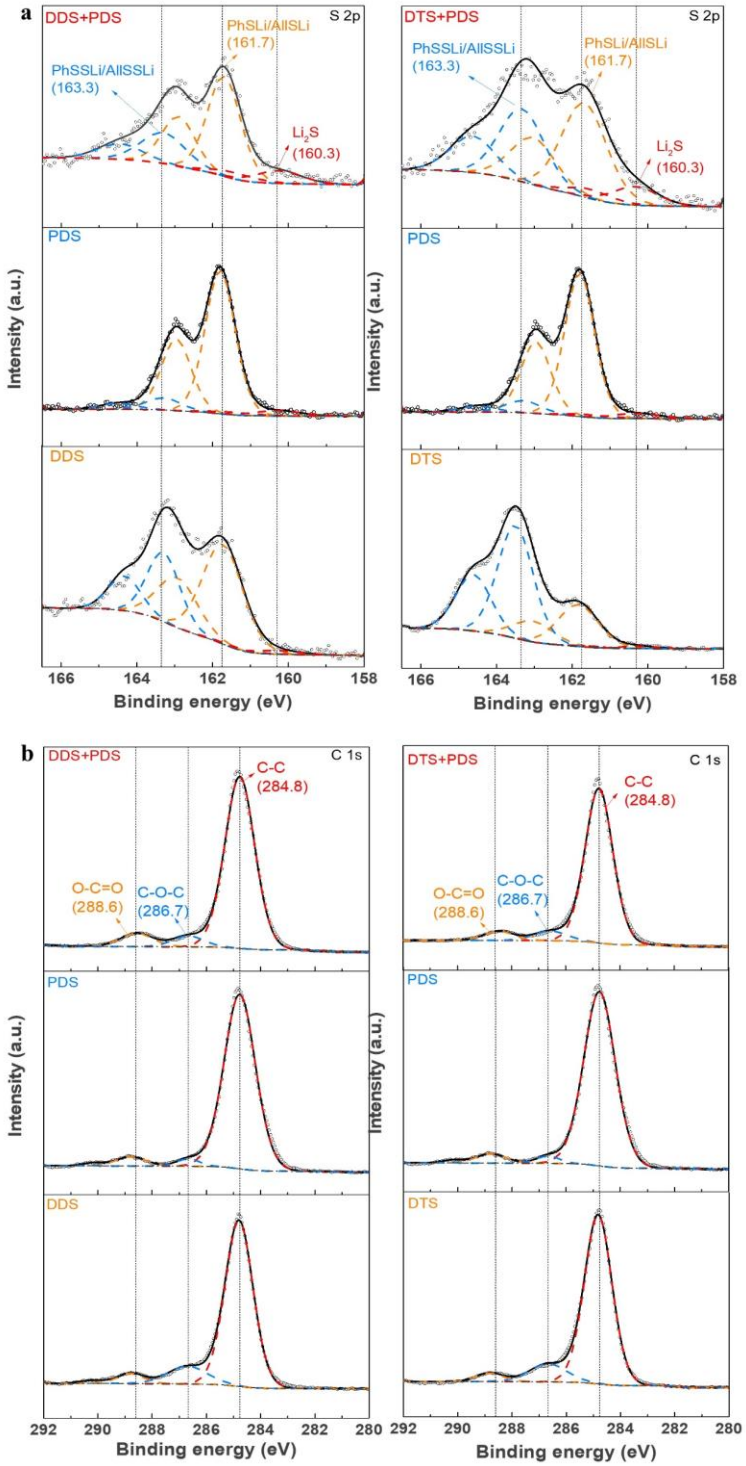

Fig. S8. XPS of the discharged sample at 1.7 V versus Li/Li$^+$. a, S 2p region of DDS+PDS, DTS+PDS, pure PDS, pure DDS and pure DTS. **b**, C 1s region of DDS+PDS, DTS+PDS, pure PDS, pure DDS and pure DTS.

Discussion of Fig. S8: X-ray photoelectron spectroscopy (XPS) was conducted to identify whether Li_2S is produced in the discharged process for DDS- and DTS-mixed systems. Supplementary Fig. 8a shows that for pure PDS, a pair of S $2p_{3/2}$ and S $2p_{1/2}$ dual peaks is observed at 161.7 eV and 162.9 eV, which is ascribed to PhSLi, the reduction product of PDS[8, 9]. Pure DDS shows two S $2p_{3/2}$ peaks at 161.7 eV and 163.3 eV. According to the literature[9-11], the two peaks can be ascribed to AllSLi (A-S-Li) and AllSSLi (A-S-S-Li), which is the reduction product of DDS and DTS, respectively. Similar to DDS, DTS also exhibits two S $2p_{3/2}$ peaks, which can be attributed to AllSLi and AllSSLi. Interestingly, for DDS+PDS and DTS+PDS systems, in addition to the observed peaks in individual member (i.e. PDS, DDS and DTS), a small peak at 160.3 eV was observed, which can be attributed to Li_2S[9-11]. The XPS results support our DFT calculation that the asymmetric allyl-substituted organosulfides promote the formation of Li_2S compared to the symmetric counterpart.

The C 1s XPS spectra of different organosulfides is shown in Supplementary Fig. 8b. For C 1s, the peaks at 284.8, 286.7 and 288.6 eV are related to C-C bonds, C-O-C and O-C=O functional groups, accordingly[12, 13].

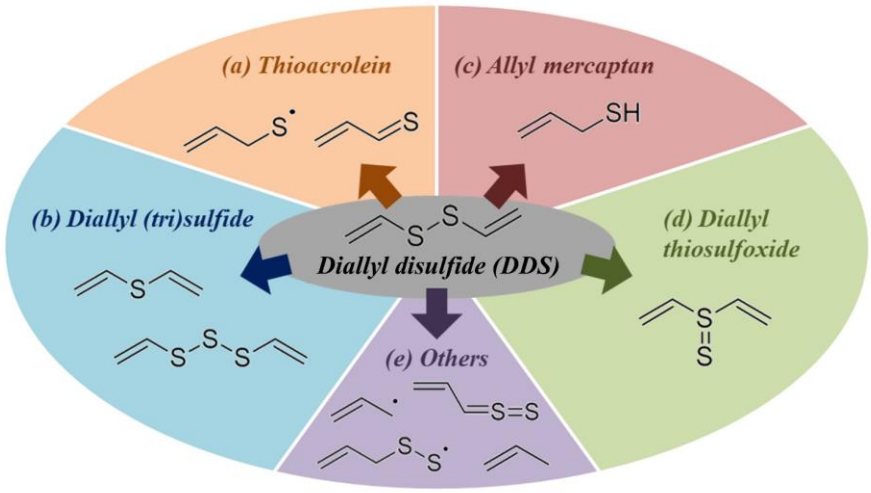

Fig. S9. Reported self-reaction products of the diallyl disulfide (DDS) molecule. a, thioacrolein. **b**, diallyl sulfide/trisulfide. **c**, allyl mercaptan. **d**, diallyl thiosulfoxide, and **e**, other species.

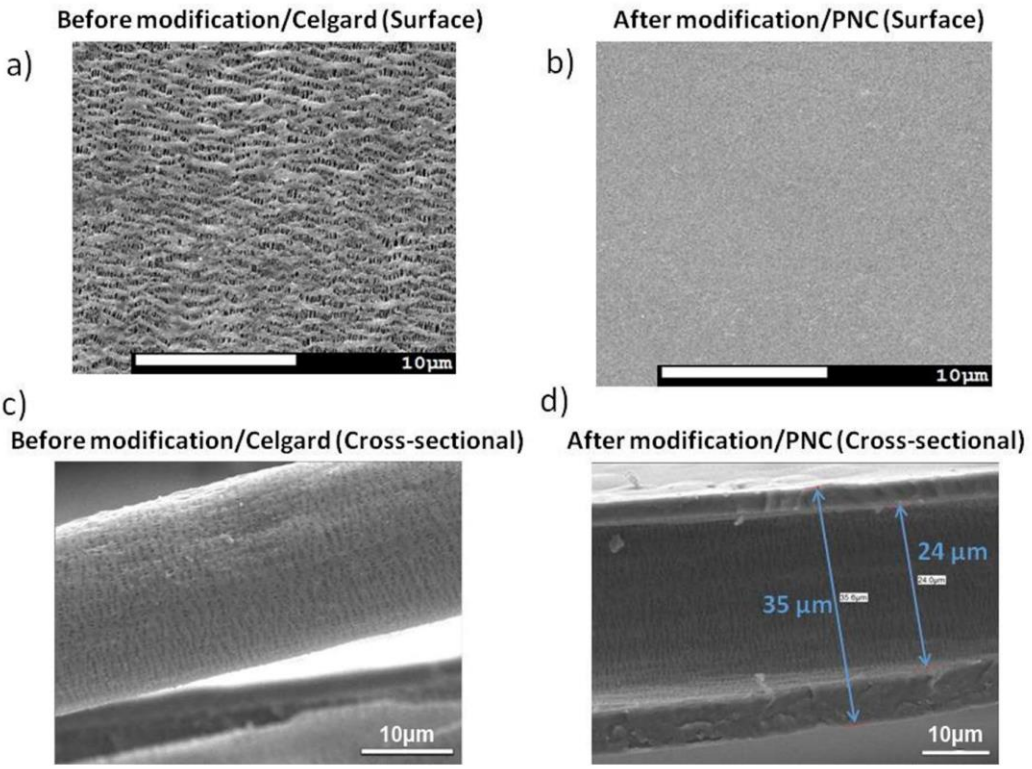

Fig. S10. SEM images of Celgard 2325 and PNC. The surface of **a)** Celargd 2325 and **b)** the PNC. The cross-sectional area of **c)** Celgard 2325 and **d)** the PNC. The scale bars are the same at 10 μm. Noted that the thickness of Celgard 2325 is about 24 μm. Samples were briefly frozen in liquid nitrogen for ~15 min and broken manually, and then dried for SEM test.

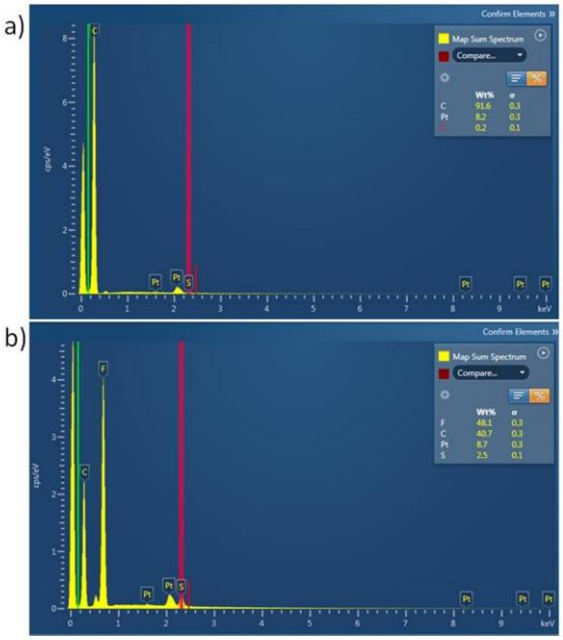

Fig. S11. EDX analysis of the surface. a, Celargd 2325. **b**, the PNC. It is clearly seen that elements of F and S are found onto the surface of the PNC while only C element is found for the case of Celgard. It is noted that Pt element was introduced during sample sputtering treatment.

Discussion of Figs. S10 and S11: As shown in Fig. S10, sandwich-like structure was observed for the PNC. The EDX analysis confirms these two polymers were successfully coated onto the surface of the Celgard (Fig. S11). This PNC is expected to reduce the crossover by size exclusion and electrostatic repulsion, while provide selective and sufficient ionic conductivity for Li^+ ions. Compared with regular polysulfide, organosulfides have bulky functional groups that could further impede the crossover process. In comparison to the commonly used membranes for nonaqueous electrochemical systems whose pretreatment (includes ion-exchange and membrane wetting) generally take 5 days to achieve good performance[14], this PNC requires very little pretreatment before use and greatly simplifies the preparation of NRFBs. We then examine the cycling stability and the Coulombic efficiency of the proposed LOB with PNC at high applied current density.

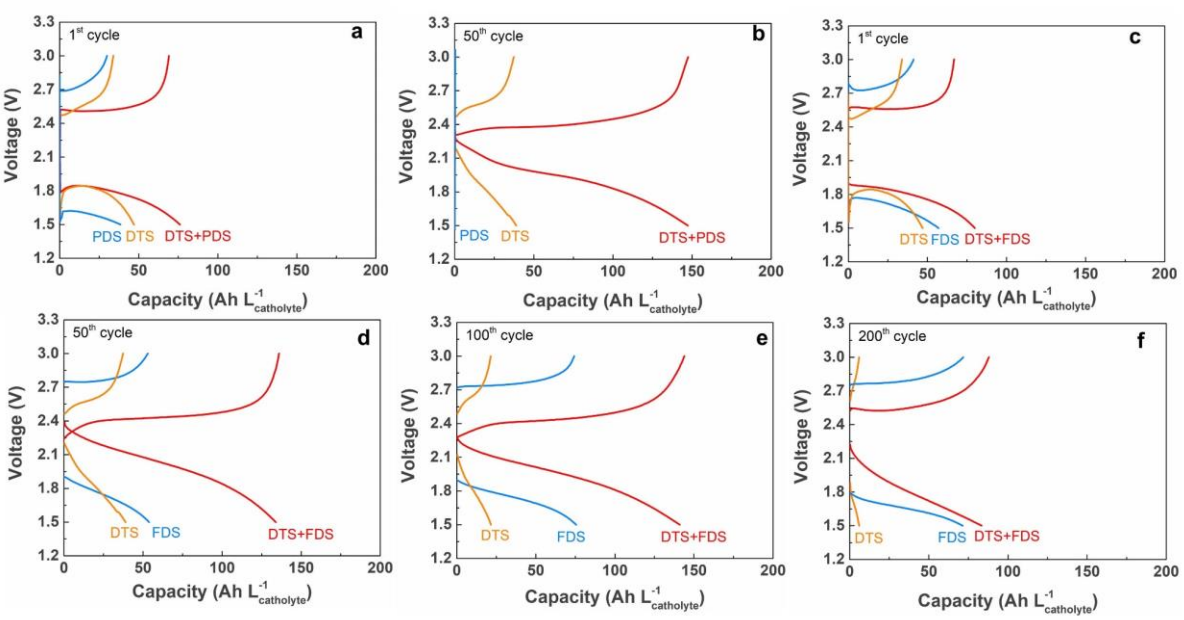

Fig. S12. Selected cycles for DTS-mixed systems (DTS+PDS and DTS+FDS) at 1 mA cm^{-2} with PNC separator from Fig.5c-d.

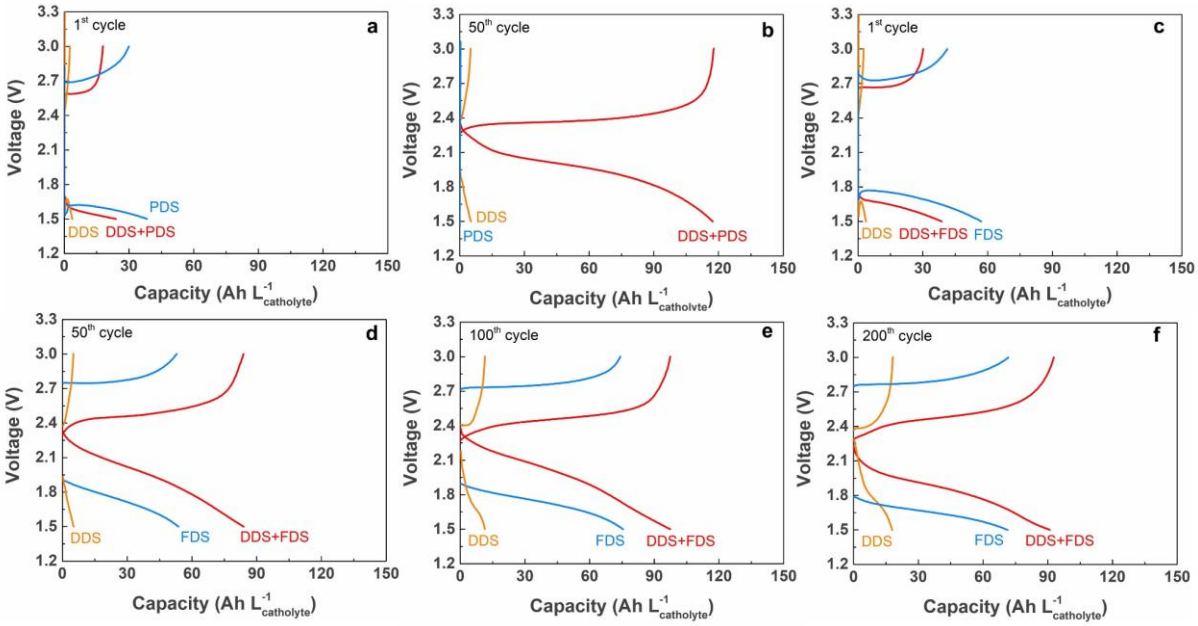

Fig. S13 Selected cycles for DDS-mixed systems (DDS+PDS and DDS+FDS) at 1 mA cm^{-2} with PNC separator from Fig.5e-f.

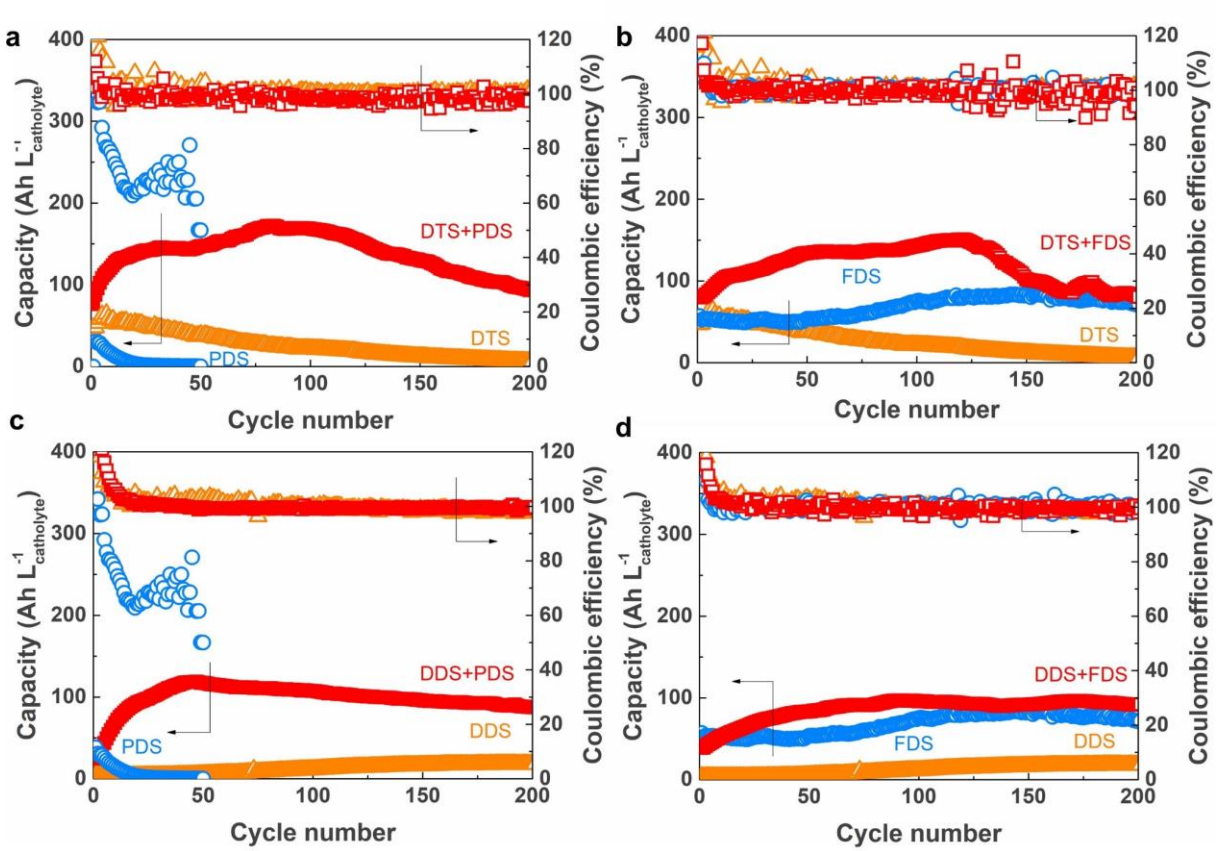

Fig. S14. Capacity and CE retention of DTS+PDS, DTS+FDS, DDS+PDS, DDS+FDS and individual system (10 µL) at 1 mA cm^{-2} with PNC separator.

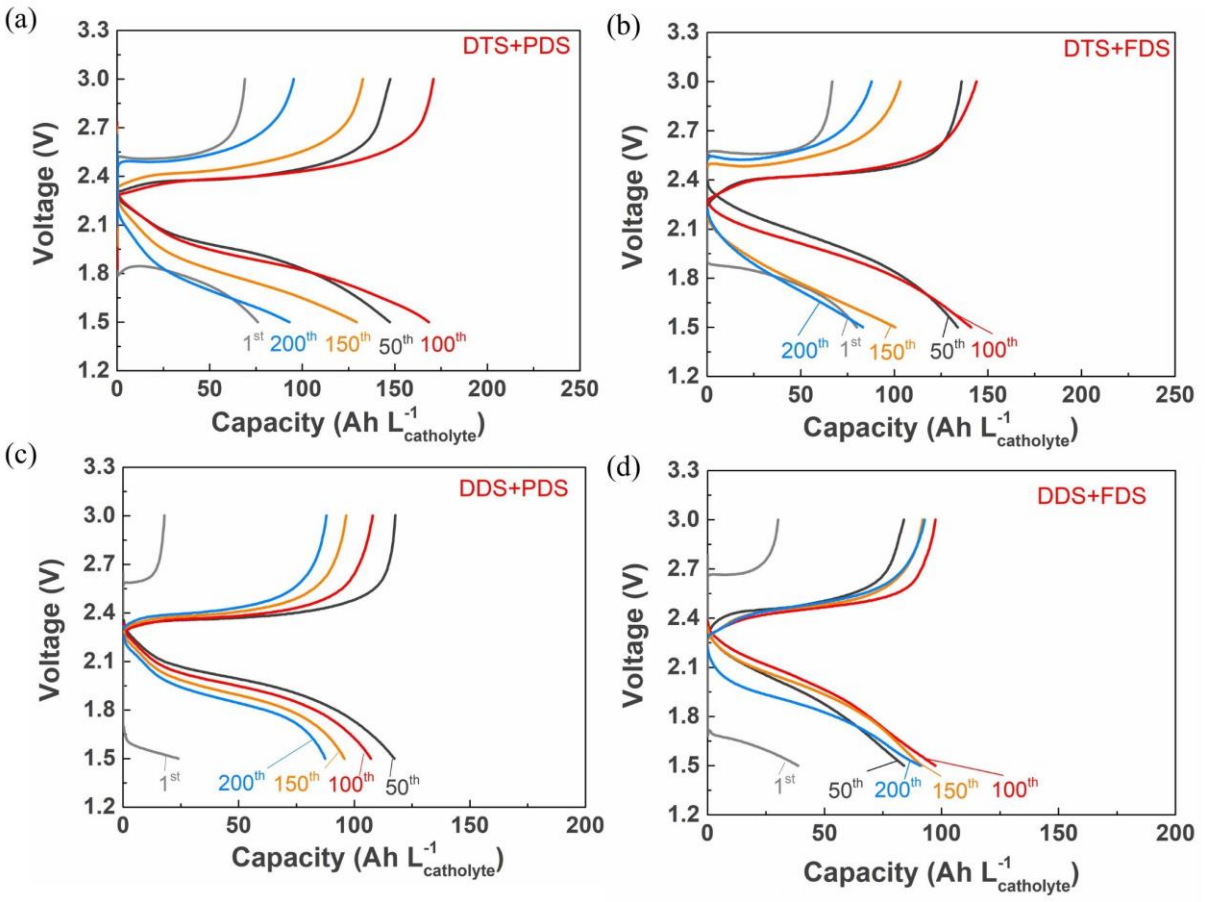

Fig. S15. Selected cycles at 1 mA cm^{-2} with PNC separator. a, DTS+PDS. **b**, DTS+FDS. **c**, DDS+PDS and **d**, DDS+FDS.

Table S3. Characteristics of the state-of-the-art redox active liquid-based catholytes for nonaqueous flow batteries.

Catholytes	Potential vs. Li/Li$^+$	Number of electron transfer	Max. demonstrated concentration (mol L^{-1})	Current density (mA cm^{-2})	Max. demonstrated capacity	Ref
Ferrocene/Ferrocenium	3.2	1	0.6	0.71	16.1	15
Acetyl ferrocene/Acetyl ferrocenium	3.65	1	0.81	0.03	21.7	16
Fc1N112-TFSI	3.49	1	0.85	3.5	22.8	17

Hydroquinone(H_2BQ/BQ)	3.4	1	0.6	3.4	17	18
Meo-TEMPO	3.6	1	2.35	1	56	19
TEMPO oxoammonium	3.5	1	2	1	36	20
$DMFc/DMFc^+$	3.15	1	3	2	68	4
$FeCp_2$	3.7	1	1	1.5	13.4*	21
LiI	3	2/3	5	2.5	65	2
$[Co(P_3O_9)_2]^{3-}/[Co(P_3O_9)_2]^{4-}$	3.95	1	0.01	0.73	0.2	22
$[Fc_4]^0/[Fc_4]^{4+}$	3.15	4	0.1	1.16	5	23
$Cu[Tf_2N]^0/Cu[Tf_2N]^+$	4.56	1	1	2.5-20	12	24
$[VBH]^{2-}/[VBH]^-$	3.1	1	0.01	NA	0.128	25
Nitronyl nitroxide	3.93	1	0.016	1	1.8	26
CP	3.6	1	0.05	0.07	1.2	27
DBMMB	4.3	1	1	10-60	2.5-3.4	28
Metallocene functionalized fullerenes	3.78	2	0.001	1-10	0.1	29
TMPD	3.2-3.8	2	0.1	0.01	NA	30
$Ni([14]aneS_4)[TFSI]_2$	4.5	1	0.3	0.05	6.25	31
Dialkoxybenzenes	4-4.2	1	0.15	5-7.5	2.5	32
Polyoxovanadate-alkoxide	3.8-4.4	1	0.01	0.01-0.1	0.07	33
Molybdenum polyoxometalates	3.4	1	0.01	0.1-0.5	NA	34
TMTD	3.36	2	0.1	5	6	35
DPTS	2.4	4	1	1.6	66	36
Polysulfide (liquid)	2.3	2	5	1.5	47	37

$LiFePO_4$	3.2	1	TMPD-targeting	0.125	320	38
Sulfur/Carbon (semi-solid)	2.5-2.0	8	20% S	4-6	294	1
EVI_2	2.5	1	PB-targeting	0.025	46.8	39
DTS+FDS (**this work**)	2.2	4	2.5	0.1	**224**	
DTS+PDS (**this work**)	2.1	4	2.5	0.1	**200**	

Notes:

* the cell capacity is limited by anolyte.

Abbreviations of active species in Supplementary Table 3.
FcN112-TFSI: ferrocenylmethyl dimethyl ethyl ammonium-bis(trifluoromethanesulfonyl)imide

Meo-TEMPO: 4-methoxy-2,2,6,6-tetramethylpiperidine 1-oxy
TEMPO oxoammonium: 2,2,6,6-tetramethylpiperidine-1-oxoammonium tetrafluoroborate
DMFc: 1,1-dimethylferrocene

$FeCp_2$: decamethylferrocenium

LiI: Lithium iodide

Fc: Ferrocene derivative

VBH: Vanadium bis-hydroxyiminodiacetate

CP: Tris(dialkylamino)cyclopropenium

DBMMB: 2,5-di-tert-butyl-1-methoxy-4-[2'-methoxyethoxy]benzene

TMPD: N,N,N',N'-tetramethyl-p-phenylenediamine

TMTD: Tetramethylthiuram disulfide

DPTS: Diphenyl trisulfide

TMPD: 2,3,5,6-tetramethyl-p-phenylenediamine

EVI_2: Ethyl viologen diiodide

PB: Prussian Blue

FDS+DTS: bis(3-fluorophenyl) disulfide + diallyl trisulfide

PDS+DTS: diphenyl disulfide + diallyl trisulfide

Supplementary References

1. H. Chen, Q. Zou, Z. Liang, H. Liu, Q. Li and Y.-C. Lu, *Nature Commun.*, 2015, **6**, 5877.
2. H. Chen and Y. C. Lu, *Adv. Energy Mater.*, 2016, 1502183.
3. G.-M. Weng, Z. Li, G. Cong, Y. Zhou and Y.-C. Lu, *Energy Environ. Sci.*, 2017, **10**, 735-741.
4. G. Cong, Y. Zhou, Z. Li and Y.-C. Lu, *ACS Energy Lett.*, 2017, **2**, 869-875.
5. G. W. T. M. J. Frisch, H. B. Schlegel, G. E. Scuseria, M. A. Robb, J. R. Cheeseman, G. Scalmani, V. Barone, G. A. Petersson, H. Nakatsuji, X. Li, M. Caricato, A. Marenich, J. Bloino, B. G. Janesko, R. Gomperts, B. Mennucci, H. P. Hratchian, J. V. Ortiz, A. F. Izmaylov, J. L. Sonnenberg, D. Williams-Young, F. Ding, F. Lipparini, F. Egidi, J. Goings, B. Peng, A. Petrone, T. Henderson, D. Ranasinghe, V. G. Zakrzewski, J. Gao, N. Rega, G. Zheng, W. Liang, M. Hada, M. Ehara, K. Toyota, R. Fukuda, J. Hasegawa, M. Ishida, T. Nakajima, Y. Honda, O. Kitao, H. Nakai, T. Vreven, K. Throssell, J. A. Montgomery, Jr., J. E. Peralta, F. Ogliaro, M. Bearpark, J. J. Heyd, E. Brothers, K. N. Kudin, V. N. Staroverov, T. Keith, R. Kobayashi, J. Normand, K. Raghavachari, A. Rendell, J. C. Burant, S. S. Iyengar, J. Tomasi, M. Cossi, J. M. Millam, M. Klene, C. Adamo, R. Cammi, J. W. Ochterski, R. L. Martin, K. Morokuma, O. Farkas, J. B. Foresman, and D. J. Fox, Gaussian 09, Revision A.1; Gaussian, Inc: Wallingford, CT, 2009.
6. R. Peverati and D. G. Truhlar, *J. Phys. Chem. Lett.*, 2011, **2**, 2810-2817.
7. A. V. Marenich, C. J. Cramer and D. G. Truhlar, *J. Phys. Chem. B*, 2009, **113**, 6378-6396.
8. A. Bhargav, S. V. Patil and Y. Fu, *Sustain. Energy Fuels*, 2017, **1**, 1007-1012.
9. W. Guo, Z. D. Wawrzyniakowski, M. M. Cerda, A. Bhargav, M. D. Pluth, Y. Ma and Y. Fu, *Chem. Eur. J.*, 2017, **23**, 16941-16947.
10. M. Wu, Y. Cui, A. Bhargav, Y. Losovyj, A. Siegel, M. Agarwal, Y. Ma and Y. Fu, *Angew. Chem., Int. Ed.*, 2016, **55**, 10027-10031.
11. S. Chen, F. Dai, M. L. Gordin, Z. Yu, Y. Gao, J. Song and D. Wang, *Angew. Chem., Int. Ed.*, 2016, **55**, 4231-4235.
12. D. G. Castner and B. D. Ratner, *Surf. Interface Anal.*, 1990, **15**, 479-486.
13. J. B. Lhoest, P. Bertrand, L. T. Weng and J. L. Dewez, *Macromolecules*, 1995, **28**, 4631-4637.
14. I. L. Escalante-García, J. S. Wainright, L. T. Thompson and R. F. Savinell, *J. Electrochem. Soc.*, 2015, **162**, A363-A372.
15. Y. Ding, Y. Zhao and G. Yu, *Nano Lett.*, 2015, **15**, 4108-4113.
16. H.-s. Kim, T. Yoon, Y. Kim, S. Hwang, J. H. Ryu and S. M. Oh, *Electrochem. Commun.*, 2016, **69**, 72-75.
17. X. Wei, L. Cosimbescu, W. Xu, J. Z. Hu, M. Vijayakumar, J. Feng, M. Y. Hu, X. Deng, J. Xiao and J. Liu, *Adv. Energy Mater.*, 2015, **5**, 1400678.
18. Y. Ding and G. Yu, *Angew. Chem. Inter. Ed.*, 2016, **55**, 4772-4776.
19. K. Takechi, Y. Kato and Y. Hase, *Adv. Mater.*, 2015, **27**, 2501-2506.
20. X. Wei, W. Xu, M. Vijayakumar, L. Cosimbescu, T. Liu, V. Sprenkle and W. Wang, *Adv. Mater.*, 2014, **26**, 7649-7653.
21. Y. Ding, Y. Zhao, Y. Li, J. B. Goodenough and G. Yu, *Energy Environ. Sci.*, 2017, **10**, 491-497.
22. J. M. Stauber, S. Zhang, N. Gvozdik, Y. Jiang, L. Avena, K. J. Stevenson and C. C. Cummins, *J. Am. Chem. Soc.*, 2018, **140**, 538-541.
23. M. Milton, Q. Cheng, Y. Yang, C. Nuckolls, R. l. Hernández Sánchez and T. J. Sisto, *Nano Lett.*, 2017, **17**, 7859-7863.
24. Y. Li, J. Sniekers, J. Malaquias, X. Li, S. Schaltin, L. Stappers, K. Binnemans, J. Fransaer and I. F. Vankelecom, *Electrochim. Acta*, 2017, **236**, 116-121.
25. H. Huang, R. Howland, E. Agar, M. Nourani, J. A. Golen and P. J. Cappillino, *J. Mater. Chem. A*, 2017, **5**, 11586-11591.
26. T. Hagemann, J. Winsberg, B. Häupler, T. Janoschka, J. J. Gruber, A. Wild and U. S. Schubert, *NPG Asia Mater.*, 2017, **9**, e340.

27. K. H. Hendriks, S. G. Robinson, M. N. Braten, C. S. Sevov, B. A. Helms, M. S. Sigman, S. D. Minteer and M. S. Sanford, *ACS Cent. Sci.*, 2018, **4**, 189–196.
28. W. Duan, J. Huang, J. A. Kowalski, I. A. Shkrob, M. Vijayakumar, E. Walter, B. Pan, Z. Yang, J. D. Milshtein and B. Li, *ACS Energy Lett.*, 2017, **2**, 1156-1161.
29. J. Friedl, M. A. Lebedeva, K. Porfyrakis, U. Stimming and T. W. Chamberlain, *J. Am. Chem. Soc.*, 2017, **140**, 401–405.
30. P. Jungjin, Y. Byeong-Chul, P. J. Sun, C. J. Wook, K. Chunjoong, S. Yung-Eun and G. J. B., *Adv. Energy Mater.*, 2017, **7**, 1602567.
31. S. Hwang, H.-s. Kim, J. H. Ryu and S. M. Oh, *Electrochem. Commun.*, 2017, **85**, 36-39.
32. J. Zhang, Z. Yang, I. A. Shkrob, R. S. Assary, B. Silcox, W. Duan, J. Zhang, C. C. Su, B. Hu and B. Pan, *Adv. Energy Mater.*, 2017, **7**, 1701272.
33. L. E. VanGelder, A. M. Kosswattaarachchi, P. L. Forrestel, T. Cook and E. Matson, *Chem. Sci.*, 2018, **9**, 1692-1699.
34. J.-J. J. Chen and M. A. Barteau, *Journal of Energy Storage*, 2017, **13**, 255-261.
35. C. Wang, Q. Lai, P. Xu, X. Li and H. Zhang, *Chin. Chem. Lett.*, 2017, **29**, 716-718
36. M. Wu, A. Bhargav, Y. Cui, A. Siegel, M. Agarwal, Y. Ma and Y. Fu, *ACS Energy Letters*, 2016, **1**, 1221-1226.
37. Y. Yang, G. Zheng and Y. Cui, *Energy Environ. Sci.*, 2013, **6**, 1552-1558.
38. Y. G. Zhu, Y. Du, C. Jia, M. Zhou, L. Fan, X. Wang and Q. Wang, *J. Am. Chem. Soc.*, 2017, **139**, 6286-6289.
39. L. Fan, C. Jia, Y. G. Zhu and Q. Wang, *ACS Energy Lett.*, 2017, **2**, 615-621.